IEEJ Transactions on Industry Applications
Vol.134 No.1 pp.1–8 DOI: 10.1541/ieejias.134.1

Paper

Radial Force Control of IPMSM Considering Fundamental Magnetic Flux Distribution

Masato Kanematsu*a) Student Member, Takayuki Miyajima* Student Member
Hiroshi Fujimoto* Senior Member, Yoichi Hori* Fellow
Toshio Enomoto** Non-member, Masahiko Kondou** Non-member
Hiroshi Komiya** Non-member, Kantaro Yoshimoto** Member
Takayuki Miyakawa** Non-member

(Manuscript received January 23, 2011, revised March 15, 2011)

This paper proposes an optimal d-axis current to suppress the 2nd radial force, which is caused by the fundamental permanent flux. Under the no-load condition, the flux distribution is approximated in order to calculate the radial force. Considering the cyclic nature of 3-phase, the optimal d-axis current reference to suppress the 2nd radial force is derived. Simulations and experiments under both load and no-load conditions are performed to demonstrate the validity of the proposed optimal d-axis current reference.

Keywords: IPMSM, maxwell stress, radial force control, radial force, flux distribution, vibration suppression

1. Introduction

IPMSMs (Interior Permanent Magnet Synchronous Motors) are widely applied in many industrial applications. In these applications, it is essential to reduce the noise and vibration. Compared with other types of electrical machine, such as induction motor and switched reluctance motor, IPMSMs are relatively quiet. However, in applications, such as industrial servos, consumer products, and automotive drives, acoustic noise and vibration are important issues. Quietness enhances high commodity value of IPMSMs. Moreover the less weight IPMSMs become because of efficient vehicle (1), the larger noise and vibration have been caused.

In IPMSMs, a strong electromagnetic force exists between the rotor magnets and the stator teeth, having components in both the tangential and radial directions. The tangential force results in torque ripple. The radial force which is stronger than the tangential force induces mechanical deformation and vibration of the stator. The causes of noise and vibration in PMSMs are investigated in (2). In (3) the relationship between skew and radial force vibration is examined. In (4) and (5), vibration caused by radial force is examined with structual analysis. In (6), with FEA (Finite Element Analysis) and experiments, a detailed study of the vibration is performed. Some relationships between vibration and structual characteristics are shown in (7) and (8). Some papers such as References (7) and (8) propose radial force reduction using structural changes. On the other hand, few methods to suppress vibration using current control are proposed. Reference (9) proposes radial force reduction with current control in condition of no-tooth effect. However this method is not versatile because the Reference (9) does not consider tooth effect and the relationship between current reference and radial force is obscure. Therefore, simpler methods which predict and reduce amplitude of radial force are required.

The radial force which is caused by the permanent magnet is mainly electrical 2nd order. This paper proposes an optimal d-axis current to suppress the 2nd radial force. The flux distribution on the no-load condition is approximated as a series of rectangle. Based on the approximate model, the radial forces on each tooth are calculated. Considering cyclic nature of 3-phase, the optimal d-axis current is derived. Second, q-axis influence is investigated with FEA. Finally, simulations and experiments under load and no-load conditions are performed to demonstrate the validity of the proposed optimal d-axis current reference.

2. Model and Maxwell Stress

2.1 *dq* Model of IPMSM

The voltage equation of IPMSM in dq-axis and the motor torque T are represented by

$$\begin{bmatrix} v_d \\ v_q \end{bmatrix} = \begin{bmatrix} L_d s + R & -\omega_e L_q \\ \omega_e L_d & L_q s + R \end{bmatrix} \begin{bmatrix} i_d \\ i_q \end{bmatrix} + \omega_e \Psi_a \begin{bmatrix} 0 \\ 1 \end{bmatrix}, \quad (1)$$

$$T = K_{mt} i_q + K_{rt} i_d i_q, \quad (2)$$

a) Correspondence to: Masato Kanematsu. E-mail: kanematsu@hflab.k.u-tokyo.ac.jp
* The University of Tokyo, 5-1-5 Kashiwanoha Kashiwa Chiba, Japan
** Nissan Motor Co., LTD., 1-1 Morinosato Aoyama Atsugi Kanagawa, Japan

$$\omega_m = \frac{1}{Js + D}T, \quad \omega_e = P\omega_m, \tag{3}$$

where $v_{d,\ q}$ are the d-axis and q-axis voltages, $i_{d,\ q}$ are the d-axis and q-axis currents, $L_{d,\ q}$ are the d-axis and q-axis inductances, R is the stator winding resistance, ω_e is the electric angular velocity, Ψ_a is the back EMF constant, $K_{mt} := P\Psi_a$, $K_{rt} := P(L_d - L_q)$, P is the number of pole pairs, and J is the rotor innertia. In this paper, 2-phase/3-phase transform is absolute transformation.

2.2 The Electromagnetic Forces of IPMSM φ_m refers to the stator position angle between the center of a U-phase tooth and a point where maxwell stress is considered. Using the definition of Maxwell stress tensor, the radial and tangential electromagnetic forces are calculated as

$$f_r(\varphi_m) = \frac{B_r^2(\varphi_m) - B_\theta^2(\varphi_m)}{2\mu_0}, \tag{4}$$

$$f_\theta(\varphi_m) = \frac{B_r(\varphi_m)B_\theta(\varphi_m)}{\mu_0}, \tag{5}$$

where $B_r(\varphi_m)$ and $B_\theta(\varphi_m)$ are the radial and tangential flux densities on φ_m, $f_r(\varphi_m)$ and $f_\theta(\varphi_m)$ are the radial and tangential maxwell stress on φ_m. In (4), $B_\theta^2(\varphi_m)$ is much smaller than $B_r^2(\varphi_m)$ and (4) can be approximated as

$$f_r(\varphi_m) = \frac{B_r^2(\varphi_m)}{2\mu_0}. \tag{6}$$

In this paper, the radial force $F_{rU,rV,rW}$ acting on the surfaces of U, V and W-phase teeth are defined as

$$F_{rU,rV,rW} = \iint f_r(\varphi_m)\mathrm{d}S, \tag{7}$$

where S is the internal surface area on a tooth.

3. Approximate Model of Flux Distribution

In this paper, the radial force is calculated using the proposed approximate flux distribution model. In this chapter, the radial flux distribution is derived. JMAG (electromagnetic field analysis software with the FEA) produced by JSOL Corporation is applied to this analysis. In FEA, it is supposed that ideal sinusoidal current flows.

3.1 Hypotheses for Approximation This paper considers 12 poles 18 slots IPMSM. The winding pattern is concentrated winding.

The value of $B_r(\varphi_m)$ is a function of i_d, i_q, φ_m, and θ_e, where θ_e is rotor angle. Moreover, it is assumed that the radial flux density $B_r(\varphi_m)$ is expressed as

$$B_r(\varphi_m) = B_{ri_d}(\varphi_m, i_d) + B_{ri_q}(\varphi_m, i_q) + B_{rm}(\varphi_m), \tag{8}$$

where, $B_{ri_d}(\varphi_m, i_d)$ and $B_{ri_q}(\varphi_m, i_q)$ are the radial flux densities due to i_d and i_q on φ_m, $B_{rm}(\varphi_m)$ is the radial flux density which is generated by the permanent magnet on φ_m. Firstly, in order to consider no-load condition, this paper neglects $B_{ri_q}(\varphi_m, i_q)$. The effect of q-axis current is described at Section 4.4.

In this paper, the linearity between i_d and $B_{ri_d}(\varphi_m)$ is assumed.

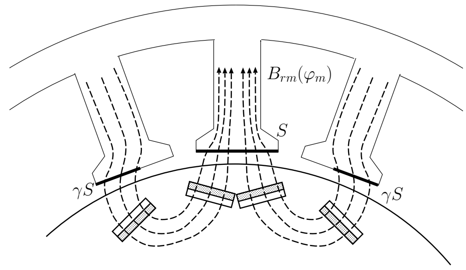

(a) Magnetic flux lines

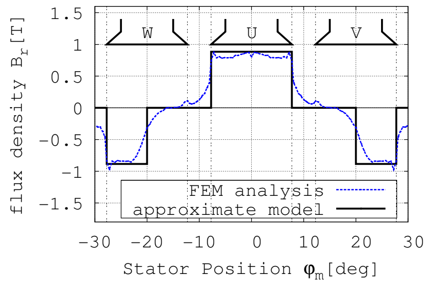

(b) $B_{rm}(\varphi_m)$

Fig. 1. Flux distribution $B_{rm}(\varphi_m)$ by permanent magnet

3.2 Approximate Model of Flux Distribution by Permanent Magnet The FEA result of the flux distribution of the permanent magnet at $\theta_e = 0$ Deg. is shown in Fig. 1(b). As shown in Fig. 1(b), the flux distribution is nearly flat on the U-phase tooth, but unequal on the V-phase and the W-phase teeth. Here, the flux distribution is approximated by a rectangle. The magnetic flux passes through the area γS and no magnetic flux passes through the other area $(1-\gamma)S$. γ $(0 < \gamma \leq 1)$ is flux interlinkage area. It is expected that γ depends on the rotor structure, but this relationship is inevident. In this paper, γ is determined from FEA, such that $\gamma = 1$ on U-phase and $\gamma = 0.5$ on V-phase and W-phase.

The fluxes $\phi_{mU,mV,mW}$ on a tooth surface are calculated as

$$\phi_{mU} = \phi, \quad \phi_{mV,mW} = -\frac{1}{2}\phi, \tag{9}$$

where N is the number of commutating turns per a tooth and $\phi := \sqrt{\frac{2}{3}}\frac{\Psi_a}{PN}$. Here, $\sqrt{\frac{2}{3}}$ is the coefficient to transform 2-phase into 3-phase.

The flux distribution of the permanent magnet is approximated as $B_{rmj} = \frac{\phi_{mj}}{S_j}$, where B_{rmj} is the flux distribution of the j-phase teeth by the permanent magnet, ϕ_{mj} is whole magnetic flux of the j-phase teeth, S_j is interlinkage flux area on the j-phase teeth. Fig. 1(b) shows the approximate model of the flux distribution.

3.3 Approximate Model of Flux Distribution by *d*-axis Current Under the assumption of Section 3.1, $B_{ri}(\varphi_m)$ is calculated by the diffenrence be-

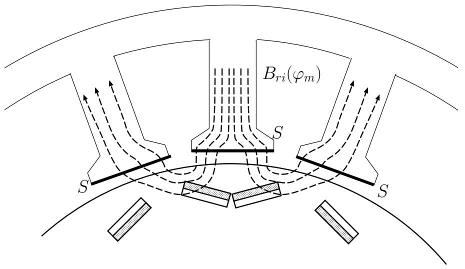

(a) Magnetic flux lines

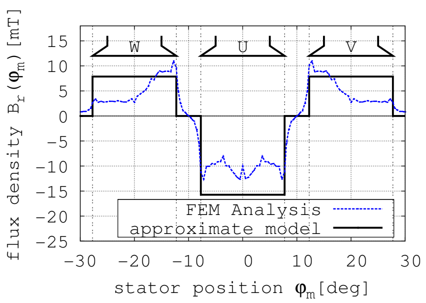

(b) $B_{ri}(\varphi_m)$

Fig. 2. Flux distribution $B_{ri}(\varphi_m)$ by d-axis current

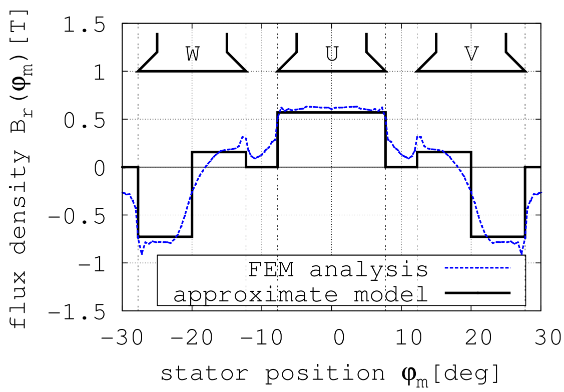

Fig. 3. Magnetic field analysis and flux approximation of $B_r(\varphi_m)$ ($i_d = -20$ [A])

tween B_r as $i_d = -1$[A] and by $B_{rm}(\varphi_m)$. Fig. 2 shows the flux distribution of $B_{ri}(\varphi_m)$ at $\theta_e = 0$ Deg. The flux distribution on the U-phase tooth is nearly flat. On the other hand, the flux distribution on the V-phase and W-phase teeth concentrate in side of the U-phase teeth. In order to obtain simple approximation model, the flux distributions on the V-phase and the W-phase teeth are regarded as flat.

$$\phi_{iU} = l_d i_d, \quad \phi_{iV,iW} = -\frac{1}{2} l_d i_d \qquad (10)$$

where $\phi_{iU,iV,iW}$ are fluxes on U-phase, V-phase and W-phase teeth by d-axis current. Here, $l_d := \sqrt{\frac{2}{3}} \frac{L_d}{PN}$.

Fig. 3 shows the flux distribution by FEA and proposed approximate model.

Table 1. IPMSM parameter

Stator Configuration	Concentrated winding
interlinkage area coefficient γ	0.5
d-axis 1-teeth inductance l_d	53.1 [μH]
turn number N	20
teeth area S	4.13×10^{-4} [m^2]
1-teeth magnetic flux ϕ	3.65 [mWb]

4. Radial Force Approximation Using Flux Distribution

4.1 Radial Force on U-phase Tooth

Fig. 4(a) shows the flux distibution image on the U-phase tooth. The flux distribution $B_r(\varphi_m)$ on the U-phase tooth is calculated as follows:

$$B_r(\varphi_m) = \left(\frac{\phi}{S} + \frac{l_d i_d}{S}\right) \qquad (11)$$

By substituting (6) and (11) into (7), (12) is obtaind.

$$\begin{aligned} F_{rU} &= \int\int f_r(\varphi_m)\mathrm{d}S \\ &= \frac{B_r^2(\varphi_m)}{2\mu_0} \cdot S \\ &= \frac{(\phi + l_d i_d)^2}{2\mu_0 S} \end{aligned} \qquad (12)$$

4.2 Radial Forces on V and W-phase Teeth

The flux distribution of the permanent magnet is not flat on the V-phase and W-phase teeth. Therefore, approximate model is derived in two areas. Fig. 4(b) shows the flux distibution image on the V-phase and the W-phase teeth. The flux distribution $B_r(\varphi_m)$, $B_r'(\varphi_m)$ and the radial force F_{rV}, F_{rW} on the V-phase and the W-phase teeth at $\theta_e = 0$ Deg. are calculated as

$$B_r(\varphi_m) = \left(\frac{\phi}{2\gamma S} + \frac{l_d i_d}{2S}\right) \qquad (13)$$

$$B_r'(\varphi_m) = \frac{l_d i_d}{2S} \qquad (14)$$

$$\begin{aligned} F_{rV}, F_{rW} &= \int\int f_r(\varphi_m)\mathrm{d}S \\ &= \frac{{B_r}^2(\varphi_m)}{2\mu_0} \cdot \gamma S + \frac{{B_r'}^2(\varphi_m)}{2\mu_0} \cdot (1-\gamma)S \\ &= \frac{(\phi + l_d i_d)^2 + \frac{(1-\gamma)}{\gamma}\phi^2}{8\mu_0 S} \end{aligned} \qquad (15)$$

4.3 Current Reference Method to Suppress Radial Force

In this section, d-axis current reference is derived to suppress the 2nd order radial force. $F_{rU}(\theta_e), F_{rV}(\theta_e)$, and $F_{rW}(\theta_e)$ refer to the radial forces of U-phase, V-phase and W-phase teeth when rotor electrical angle is θ_e. When θ_e is 0 or π rad., the radial force on U-phase tooth is maximum and equal to $F_{rU}(0)$, which is obtained in (12). The radial force on U-phase tooth is minimum when θ_e is $\frac{1}{2}\pi$ or $\frac{3}{2}\pi$ rad. At this point, it is difficult to approximate radial force because the flux which does not interlink exists. Therefore, the radial force $F_{rU}(\frac{\pi}{3})$ is used instead of $F_{rU}(\frac{\pi}{2})$. When

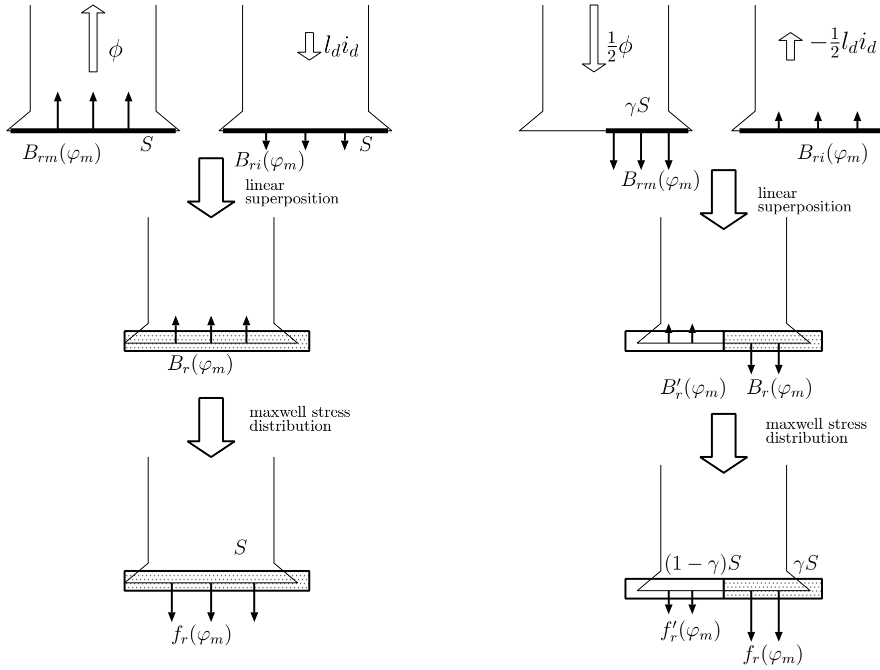

(a) Flux distribution image on U-phase (b) Flux distribution image on V and W-phase

Fig. 4. Radial force calculation

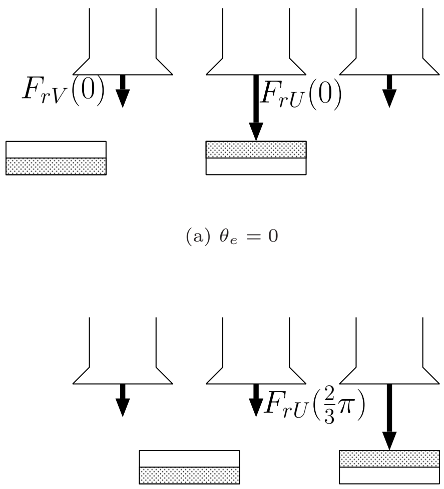

(a) $\theta_e = 0$

(b) $\theta_e = \frac{2}{3}\pi$

Fig. 5. The positions of teeth and magnet

three-phase equilibrium is correct in IPMSM, $F_{rU}(\frac{2}{3}\pi)$ equals $F_{rV}(0)$. In Fig. 5, the physical relationships between teeth and magnet when θ_e changes are shown. $F_{rV}(0)$ is approximated in (15). Moreover, by cyclic nature, $F_{rU}(\theta_e)$ has the equal values at electrical angle $\theta_e = \frac{1}{3}\pi, \frac{2}{3}\pi, \frac{4}{3}\pi, \frac{5}{3}\pi$[rad]. Therefore, when the following equation is true, it is predicted that 2nd radial force is suppressed largely.

$$F_{rU}(0) = F_{rU}\left(\frac{2}{3}\pi\right) \tag{16}$$

As the equations (12) and (15) are functions for i_d, we can select a d-axis current reference to satisfy the equation (16). From (12), (15), and (16), the optimal d-axis current which achieves minimum 2nd order radial force is represented by

$$i_{d:\mathrm{opt}} = \left(-1 \pm \sqrt{\frac{1-\gamma}{3\gamma}}\right)\frac{\phi}{l_d}. \tag{17}$$

By taking into the consideration of $0 < \gamma \leq 1$, $i_{d:\mathrm{opt}}$ is real number. Here, plus sign in (17) is selected in order to use minimum current amplitude. Using Table. 1, $i_{d:\mathrm{opt}}$ is calculated by

$$i_{d:\mathrm{opt}} = -29.1\mathrm{A}. \tag{18}$$

4.4 The Influence of Flux Distribution by q-axis Current In this section, the influence of flux distribution attributed by q-axis current is considered. The FEA result of the flux distribution by q-axis current is shown in Fig. 6. Fig. 6 shows that the flux distribution on U-phase tooth is 0. The dq/3-phase transform matrix $\boldsymbol{C}_{UVW}^{dq}$ at $\theta_e = 0$ is given by

$$\boldsymbol{C}_{UVW}^{dq} = \sqrt{\frac{2}{3}}\begin{bmatrix} 1 & 0 \\ -\frac{1}{2} & \frac{\sqrt{3}}{2} \\ -\frac{1}{2} & -\frac{\sqrt{3}}{2} \end{bmatrix}. \tag{19}$$

This means the flux by q-axis current passes only through the V-phase and the W-phase teeth. In Fig. 6, the magnetic flux and the q-axis flux affect each other, and this leads to asymmetry of the flux distribution on the V-phase and W-phase teeth.

4.5 Verification of Radial Force Estimate Equation In this section, the accuracy of the op-

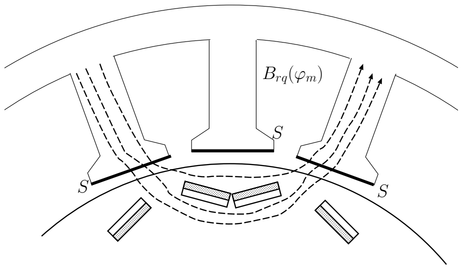

(a) Magnetic flux lines

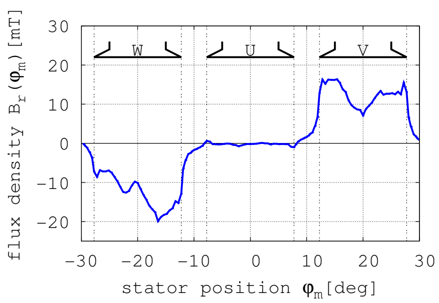

(b) $B_{ri_q}(\varphi_m)$

Fig. 6. Flux distribution $B_{ri_q}(\varphi_m)$ by q-axis current

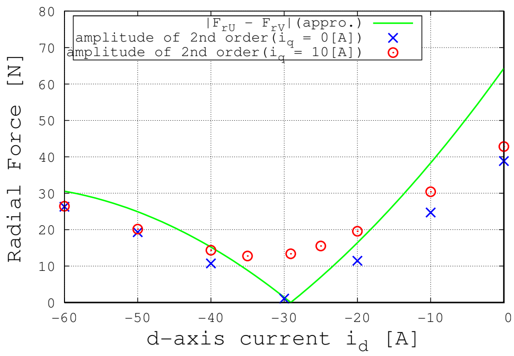

Fig. 7. Comparison with approximate radial force and analysis data

timal d-axis current reference is validated. The difference between $F_{rU}(0)$ and $F_{rU}(\frac{2}{3}\pi)$ is proportional to the amplitude of 2nd radial force. In Fig. 7, $\left|F_{rU}\left(0\right) - F_{rU}\left(\frac{2}{3}\pi\right)\right|$ and 2nd radial force analyzed by FEA are shown on no-load and load conditions. The 2nd radial force is minimized by the optimal d-axis current reference on each condition. On load condition, 2nd radial force at $i_{d:\mathrm{opt}}$ cannot be reduced to 0 by d-axis current because the remaining radial force is caused by q-axis current. Fig. 7 shows the d-axis current reference $i_{d:\mathrm{opt}}$ which is calculated on no-load condition is helpful to reduce the 2nd radial force on load condition. Fig. 8 shows the time waveforms when $i_{d:\mathrm{opt}}$ is 0 A and -29.1 A on each condition. Fig. 8(a) and 8(b) show that (17) is an optimal reference to suppress the radial force vibration. 2nd radial forces are suppressed by over 95 % in no-load condition, by over 60 % in load condition in Fig. 8(d).

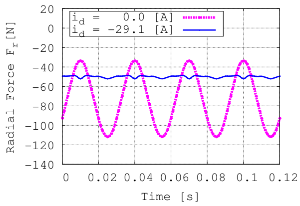

(a) $i_q = 0$ A(no load condition)

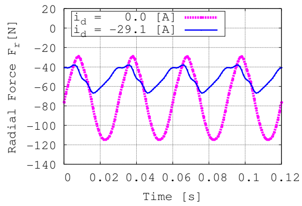

(b) $i_q = 10$ A(load condition)

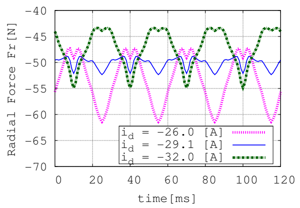

(c) $i_q = 0$ A(detail)

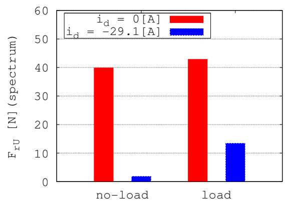

(d) 2nd order spectrum of radial force

Fig. 8. U-phase radial force F_{rU} suppression with d-axis current

5. Experiment

It is difficult to measure the radial force directly. In this paper, the radial accerelation outside the stator is evaluated instead of the radial force.

The experimental results at 1500 rpm(f_e = 150 Hz) are shown in Fig. 9. Here, horizontal axis is the frequency normalized by electric angle frequency f_e. In this paper, the negative d-axis current reference is limited within -25 A because of the motor rating. Fig. 9(a) and 9(b) show the 2nd order acceleration on load condition is slightly larger than that on no-load condition. This result corresponds to FEA result as shown in Fig. 8(d). 2nd order acceleration on load condition is less reductive by d-axis current than that on no-load condition in Fig. 9(g) and 9(h). In no-load and load conditions, the radial forces of 2nd order are largely suppressed by the d-axis current.

Fig 10 shows the change of amplitude of 2nd acceleration. In each condition, 2nd accelerations are largely decreased. Amplitude of 2nd acceleration on load condition is larger than that on no-load condtion.

6. Conclusion

In this paper, an optimal d-axis current reference which reduces 2nd radial force is proposed. The relationship between d-axis current and 2nd radial force is examined. The approximate model of the 2nd radial force predicts and controls the amplitude of 2nd radial acceleration. Experiments are performed to demonstrate the validity of this modeling. In automotive applications, IPMSMs use wide range of rotation speed, and the noise and vibration cause serious problem when the frequency of 2nd radial force corresponds to the frequency of res-

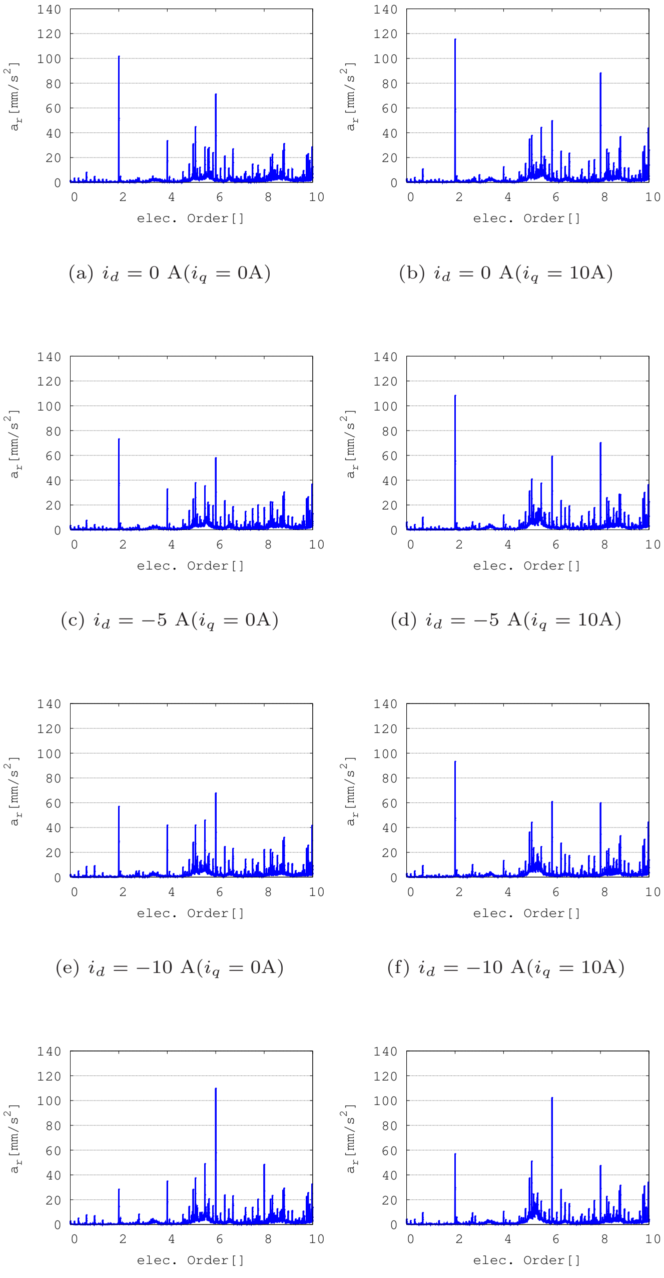

(a) $i_d = 0$ A($i_q = 0$A) (b) $i_d = 0$ A($i_q = 10$A)

(c) $i_d = -5$ A($i_q = 0$A) (d) $i_d = -5$ A($i_q = 10$A)

(e) $i_d = -10$ A($i_q = 0$A) (f) $i_d = -10$ A($i_q = 10$A)

(g) $i_d = -25$ A($i_q = 0$A) (h) $i_d = -25$ A($i_q = 10$A)

Fig. 9. Experimental Results a_r spectrum

onant frequency of the stator. In this rotation speed, it is useful to reduce motor vibration with injecting the optimal d-axis current although the motor efficiency decreases temporarily.

The amplitude of high order radial force is smaller than that of 2nd radial force. However, high order radial force, specially 6th order, can easily transmit stator and generate large acceleration when rotating speed equals stator natural frequency. In our future work, high order radial force modeling and control method will be realized.

References

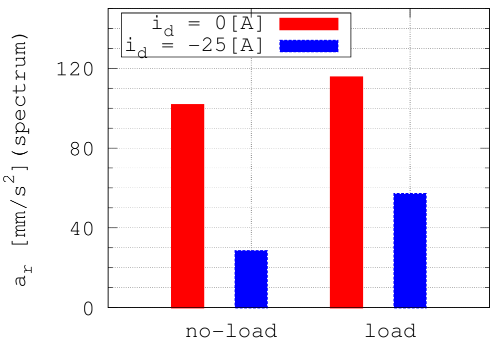

Fig. 10. 2nd order spectrum of radial acceleration

(1) Kondo Keiichiro,Kubota Hisao: "Innovative Application Technologies of AC Motor Drive Systems" IEEJ Trans. Industry Applications, Vol.1, No.3 pp.132-140(2012)

(2) J.F. Gieras, Chong Wang, Joseph. C.S.Lai, Nesimi Ertugrul: "Analytical Prediction of Noise of Magnetic Origin Produced by Permanent Magnet Brushless Motors," IEEE International Conference on Electric Machines Drives Conference(IEMDC), Vol.1, No.5, pp.148-152(2007)

(3) Jae-Woo Jung, Do-Jin Kim, Jung-Pyo Hong, Geun-Ho Lee, Seong-Min Jeon: "Experimental Verification and Effects of Step Skewed Rotor Type IPMSM on Vibration and Noise," IEEE Trans. Magnetics, Vol.47, No.10, pp.3661-3664(2011)

(4) R.Islam, I.Husain : "Analytical model for predicting noise and vibration in permanent magnet synchronous motors", IEEE International Conference on Energy Conversion Congress and Exposition(ECCE), Vol.20, No.24, pp.3461-3468(2009)

(5) M.Islam, R.Islam, T.Sebastian : "Noise and vibration characteristics of permanent magnet synchronous motors using electromagnetic and structural analyses", IEEE International Conference on Energy Conversion Congress and Exposition (ECCE), Vol.17, No.22, pp.3399-3405(2011)

(6) M.Boesing, Rik W.De Doncker : "Exploring a vibration synthesis process for the acoustic characterization of electric drives", IEEE International Conference on Electrical Machines (ICEM), Vol.6, No.8, pp.1-6(2010)

(7) Tao Sun, Ji-Min Kim, Geun-Ho Lee, Jung-Pyo Hong, Myung-Ryul Choi: "Effect of Pole and Slot Combination on Noise and Vibration in Permanent Magnet Synchronous Motor", IEEE Trans. Magnetics, Vol.47, No.5, pp.1038-1041(2011)

(8) Z.Q.Zhu, Z.P.Xia, L.J.Wu, G.W.Jewell : "Analytical modelling and finite element computation of radial vibration force in fractional-slot permanent magnet brushless machines", International Conference on Electric Machines and Drives Conference(IEMDC), Vol.3, No.6, pp.144-151(2009)

(9) Jiao Guandong, C.D.Rahn : "Field weakening for radial force reduction in brushless permanent-magnet DC motors" IEEE Trans. Magnetics, Vol.40, No.5, pp. 3286- 3292(2004)

Masato Kanematsu (Student Member) received the B.S. degree in Department of Electrical and Electronic Engineering from The University of Tokyo, Tokyo, Japan, in 2012. He is currently working towards the M.S. degree in the Department of Advanced Energy, The University of Tokyo, Chiba, Japan. His research interests include motor drive and design for electric vehicle.

Mr. Kanematsu is a student member of the Institute of Electrical Engineers of Japan, the Japan Society of Mechanical Engineers, and the Society of Automotive Engineers of Japan.

Takayuki Miyajima (Student Member) received the B.S. and M.S. degrees in electrical and computer engineering from Yokohama National University, Yokohama, Japan, in 2009 and 2011, respectively. He is currently working towards the Ph.D. degree in the Department of Advanced Energy, The University of Tokyo, Chiba, Japan. His current work concerns motor drive for electric and hybrid vehicles and electric vehicle motion control.

Mr. Miyajima is a student member of the Institute of Electrical and Electronics Engineers and the Society of Automotive Engineers of Japan.

Hiroshi Fujimoto (Senior Member) received the Ph.D. degree in the Department of Electrical Engineering from the University of Tokyo in 2001. In 2001, he joined the Department of Electrical Engineering, Nagaoka University of Technology, Niigata, Japan, as a research associate. From 2002 to 2003, he was a visiting scholar in the School of Mechanical Engineering, Purdue University, U.S.A. In 2004, he joined the Department of Electrical and Computer Engineering, Yokohama National University, Yokohama, Japan, as a lecturer and he became an associate professor in 2005. He is currently an associate professor of the University of Tokyo since 2010. He received the Best Paper Award from the IEEE Transactions on Industrial Electronics in 2001, Isao Takahashi Power Electronics Award in 2010, and Best Author Prize of SICE in 2010. His interests are in control engineering, motion control, nano-scale servo systems, electric vehicle control, and motor drive. Dr. Fujimoto is a member of IEEE, the Society of Instrument and Control Engineers, the Robotics Society of Japan, and the Society of Automotive Engineers of Japan.

Yoichi Hori (Fellow) received his B.S., M.S., and Ph.D. degrees in Electrical Engineering from the University of Tokyo, Tokyo, Japan, in 1978, 1980, and 1983, respectively. In 1983, he joined the Department of Electrical Engineering, The University of Tokyo, as a Research Associate. He later became an Assistant Professor, an Associate Professor, and, in 2000, a Professor at the same university. In 2002, he moved to the Institute of Industrial Science as a Professor in the Information and System Division, and in 2008, to the Department of Advanced Energy, Graduate School of Frontier Sciences, the University of Tokyo. From 1991-1992, he was a Visiting Researcher at the University of California at Berkeley.

His research fields are control theory and its industrial applications to motion control, mechatronics, robotics, electric vehicles, etc.

Prof. Hori is the winner of the Best Transactions Paper Award from the IEEE Transactions on Industrial Electronics in 1993 and 2001, of the 2000 Best Transactions Paper Award from the Institute of Electrical Engineers of Japan (IEEJ), and 2011 Achievement Award of IEE-Japan.

He is an IEEE Fellow and a past AdCom member of IES. He has been the Treasurer of the IEEE Japan Council and Tokyo Section since 2001. He is also a member of the Society of Instrument and Control Engineers; Robotics Society of Japan; Japan Society of Mechanical Engineers; and the Society of Automotive Engineers of Japan.

He is the past- President of the Industry Applications Society of the IEEJ, the President of Capacitors Forum, and the Chairman of Motor Technology Symposium of Japan Management Association (JMA) , the Director on Technological Development of SAE-Japan (JSAE) and the Director of Japan Automobile Research Institute (JARI).

Toshio Enomoto (Non-member) was born in 1965 in Ibaraki, Japan. Since completing B.S., in Applied Physics in 1988 at Tohoku Univ., from 1988 to 1991, he worked for MAZDA Motor Co., Ltd. Since 1991, he has worked for NISSAN Motor Co., Ltd. Currently he is managing groups of noise and vibration performance, engine mounting and exhaust system.

Masahiko Kondou (Non-member) was born in 1957 in Tokyo, Japan. He received the B.S., degree from Chuo University, Tokyo, Japan, in 1981. Since 1981, he has worked for NISSAN Motor Co., Ltd.. Currently he has been developing a good noise and vibration performance for Electric Vehicles.

Hiroshi Komiya (Non-member) received the B.E, degrees in mechanical engineering from Tokyo University of Science, Japan, in 1989. Since 1989, He works as NVH development engineer in Nissan Motor Company, and a particularly, experience about Powertrain technology development are abundant. He is a member of Society of Automotive Engineer of Japan.

Kantaro Yoshimoto (Member) was born in 1975 in Yokohama, Japan. He received the B.S., M.S., and Ph.D. from Yokohama National University, Yokohama, Japan, in 1997, 1999, and 2010 respectively. From 1999 to 2000, he worked for East Japan Railway Co.,. Since 2001, he has worked for NISSAN Motor Co., Ltd.. He is performing the development of Electric Vehicles.

Takayuki Miyakawa (Non-member) was born in 1980 in Kawasaki, Japan. He received the B.E., M.E., degree from Chuo University, Tokyo, Japan, in 2003, 2005. Since 2005, he has worked for NISSAN Motor Co., Ltd.. Currently he has been developing N.V. performance for Electric Vehicles and N.V. performance of chassis.